journal of the mechanical behavior of biomedical materials 123 (2021) 104766

Contents lists available at ScienceDirect

Journal of the Mechanical Behavior of Biomedical Materials

journal homepage: www.elsevier.com/locate/jmbbm

Removal of glycosaminoglycans affects the *in situ* mechanical behavior of extrafibrillar matrix in bone

Yan Han [a], Joel Gomez [a], Rui Hua [b], Pengwei Xiao [a], Wei Gao [a], Jean X. Jiang [b,**], Xiaodu Wang [a,*]

[a] Department of Mechanical Engineering, University of Texas at San Antonio, Texas, USA
[b] Department of Biochemistry and Structural Biology, UT Health San Antonio, Texas, USA

ARTICLE INFO

Keywords:
Bone
Atomic force microscopy
Mineralized collagen fibrils
Extrafibrillar matrix
Elastic modulus
Toughness

ABSTRACT

Previous studies have shown that glycosaminoglycans (GAGs) in bone matrix, coupling with water in bone matrix, may play a significant role in toughening bone tissues. Since GAGs are most likely present only in the extrafibrillar matrix (EFM) of bone, we hypothesized that GAGs in EFM would have a major impact on bone tissue toughness. To confirm this conjecture, we removed GAGs *ex vivo* from human cadaveric bone samples using a protein deglycosylation mix kit and then examined the *in situ* mechanical behavior of mineralized collagen fibrils (MCFs) and the surrounding EFM of the samples, using a high-resolution atomic force microscopy (AFM). By testing the bone samples before and after removal of GAGs, we found that under the wet condition removal of GAGs resulted in an increase in the elastic modulus of both EFM and MCFs, whereas a significant decrease in plastic energy dissipation was observed mainly in EFM. In contrast, under the dry condition the removal of GAGs had little effects on the mechanical properties of either MCFs or EFM. These results suggest that both MCFs and EFM contribute to the plastic energy dissipation of bone, whereas in the presence of matrix water removal of GAGs significantly reduces the capacity of EFM in plastic energy dissipation, but not MCFs. In addition, GAGs may affect the elastic modulus of both EFM and MCFs. These findings give rise to new understanding to the underlying mechanism of GAGs in toughening of bone tissues.

1. Introduction

Bone is a hierarchical composite, encompassing nano to macroscopic length scales and consisting of mineral crystal (hydroxyapatite), collagen fibrils, non-collagenous proteins (NCPs), and water (Fratzl and Weinkamer, 2007; Rho et al., 1998; Weiner and Wagner, 1998). Thus, any structural changes at different hierarchies could significantly affect bulk mechanical properties of bone (Nalla et al., 2003; Wang et al., 2018). At the ultrastructural level, mineralized collagen fibrils (MCFs) are embedded in an extrafibrillar matrix (EFM), which are comprised of NCPs and extrafibrillar minerals. In addition to the collagen and mineral phases (Burr, 2002; Currey, 1984a, b; Wang, 2002; Wang et al., 2001), NCPs might also affect the tissue-level toughness of bone (Bailey et al., 2017; Hua et al., 2020; Morgan et al., 2015; Sroga and Vashishth, 2012; Wang et al., 2016).

As a major part of NCPs, proteoglycans (PGs) are comprised of a core protein covalently bonded with glycosaminoglycan (GAG) side chains (Fisher et al., 1983; Goldberg and Takagi, 1993; Iozzo and Schaefer, 2015). GAGs are highly negatively charged, thus possessing a great potential to absorb and retain water in bone matrix *via* osmotic effects (Jameson et al., 1993; Nyman et al., 2006). This feature is very important because water plays a significant role in plasticizing bone tissues. Recent evidence shows that the amount of GAGs, coupled with bound water, is significantly correlated with the toughness of bulk bone tissues (Samuel et al., 2014; Zhu et al., 2009). Moreover, aged-related deterioration of bone toughness is also reported to be associated with diminishing amount of GAGs and bound water in bone matrix (Wang et al., 2018). However, how GAGs affect mechanical properties of bone at ultrastructural levels is still unclear.

PGs/GAGs are believed to exist only in the extrafibrillar matrix (EFM) as they have a high affinity to extrafibrillar minerals, showing that mineral crystal surfaces are predominantly in contact with GAGs

* Corresponding author.
** Corresponding author.
E-mail addresses: jiangj@uthscsa.edu (J.X. Jiang), xiaodu.wang@utsa.edu (X. Wang).

https://doi.org/10.1016/j.jmbbm.2021.104766
Received 6 April 2021; Received in revised form 4 August 2021; Accepted 6 August 2021
Available online 10 August 2021

rather than any other organic components (Hashimoto et al., 1995a; Mbuyi-Muamba et al., 1989a; Wise et al., 2007). In addition, studies also suggested that proteoglycans might play a role in stabilizing the mineral surfaces and regulating mineral deposition and crystal morphology in bone (Boskey, 1992; Lamoureux et al., 2007; Wang et al., 2015). Thus, we postulate that GAGs may mainly affect the mechanical property of EFM rather than that of MCFs. Assuming that EFM is a nanocomposite of hydroxyapatite (HA) crystals bounded *via* a thin organic interface of NCPs, an *in silico* simulation study suggests that changes in the mechanical properties of the organic interface in EFM could significantly affect the mechanical properties of bone at sub-lamellar tissue levels (Maghsoudi-Ganjeh et al., 2020). However, experimental evidence that directly supports the conjecture is still lacking.

Among the currently available techniques, atomic force microscopy (AFM) is potentially capable of measuring the *in situ* mechanical behavior of MCFs and EFM at nanometer scales *via* nanoindentation tests (Garcia, 2020). In the past, investigators attempted to measure the morphology and elastic modulus of collagen fibrils using AFM (Hang and Barber, 2011; Reilly et al., 2001; Yang et al., 2018). The elastic modulus of the collagen fibril bundles was also tested by AFM nanoindentation at sub-micrometer scales (Yang et al., 2018). However, no prior study has reported the measurement of the *in situ* mechanical property of MCFs and the surrounding EFM individually using AFM techniques.

To this end, we hypothesize that coupling with water, GAGs play an important role in sustaining the toughness of bone only in EFM regions, while having limited effects on the toughness of MCFs. To test the hypothesis, we used high-resolution AFM techniques to determine changes in the *in situ* mechanical behavior of EFM and MCFs in human cadaver cortical bone under both wet and dry conditions and before and after *in vitro* enzymatic removal of GAGs from the bone matrix.

2. Materials and methods

2.1. Bone sample preparation

In this study, cortical bone specimens were prepared from the posterior aspect of mid-diaphyseal femurs from four female human donors (41–46 years old) in order to mitigate the confounding influence of age and gender to the experimental results. As shown in Fig. 1A, cortical cores with a diameter of 7 mm were firstly extracted perpendicular to the longitudinal axis of the bone using a bench-top drilling machine (Mini Vertical Milling/Drilling Machine, China). 0.5 mm thick slices were then cut from the cores using a precision low-speed diamond saw (Pico 155 precision cutter, Pace Technologies). The slices were lapped with successive grits of sand papers, and polished with 0.1 μm particles until the thickness was about 200 μm and a surface roughness less than 30 nm.

Three slices were prepared from each donor. Of the three slices, one served as a baseline control without any treatments. Another one served as a control, which was treated only by heating in a denaturing reaction buffer at 75 °C for 10 min. The last one served as GAGs removal specimen, which was first heated in a denaturing reaction buffer at 75 °C for 10 min to expose GAGs, and then treated in the enzyme solution at 37 °C for 16 h to remove GAGs. In addition, each slice was first tested under wet condition, and then was dehydrated and tested under dry condition. Three groups of bone slices from the four donors (N = 4) were tested under both wet and dry conditions in this study.

The dark osteons were selected from each slice using a polarized microscope (MJ9430, Meiji Techno, Japan) to ensure that the mineralized collagen fibrils were longitudinally oriented to facilitate AFM measurements on MCFs and EFM. In order to minimize variations induced by tissue age, only newly formed osteons, which had intact cement lines, were selected for this study. To test the bone specimens under the wet condition, a custom-designed specimen chamber was used to ensure the bone slice being hydrated from underneath by water absorbed *via* the gauze inside the hollow specimen holder (Fig. 1B). The bone specimens were wrapped in gauze soaked with PBS prior to tests to help compensate possible water loss during sample preparations, thus keeping their initial hydration status consistent. For AFM measurements under the dry condition, bone slices were dehydrated in a vacuum at 60 °C for 4 h to remove the free and bound water from the bone matrix (Nyman et al., 2006) and no water filled in the specimen chamber during the tests.

2.2. AFM imaging of mineralized collagen fibrils and extrafibrillar matrix

A single frequency AFM method, Peak Force Tapping (PeakForce QNM), was used to map the surface topography (surface height) as well as other surface properties, such as peak force error, adhesion, and

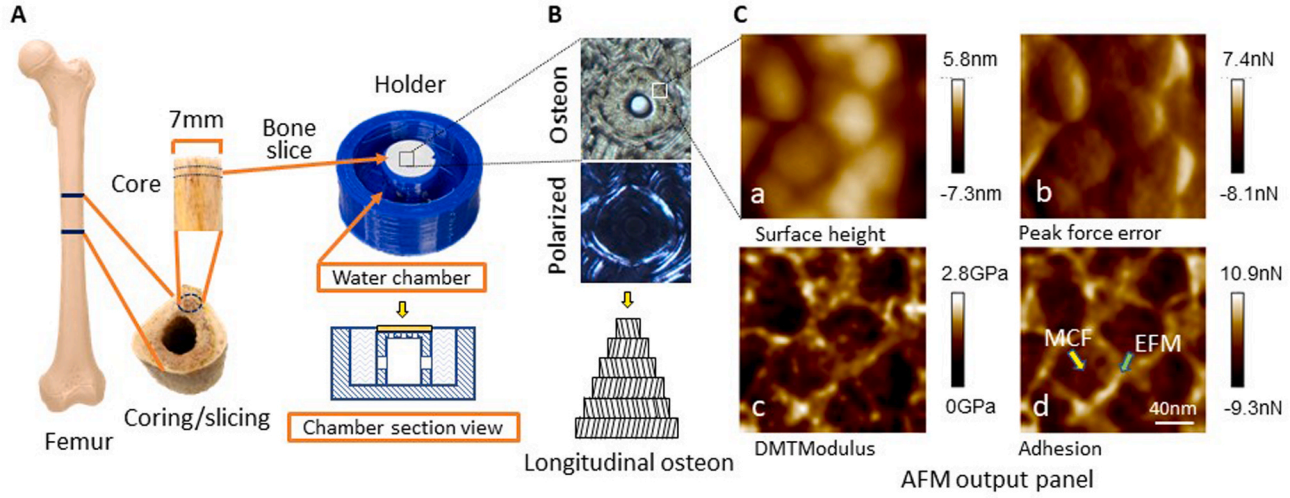

Fig. 1. Sample preparation and AFM imaging. (A) Sample preparation: bone slices (7 mm in diameter) were cut from the mid-diaphysis of femurs, and then ground and polished till the thickness was about 200 μm and a surface roughness was less than 30 nm. For AFM measurements, the bone slice was mounted onto the hollow cylindrical holder in the sample holder. For the test under the wet condition, the water chamber was filled with distilled water and the bone anchor was filled up with gauze to soak the water, thus keeping the bone slice moist. (B) The dark osteons were selected under the polarized microscope, which contain the longitudinally oriented collagen fibrils to facilitate AFM measurements and nanoindentation tests on MCFs and EFM. (C) AFM image output indicating (a) surface height; (b) surface topography; (c) surface modulus mapping; and (d) surface adhesion mapping.

DMTModulus in a high-resolution AFM system (Dimension Icon, Bruker, Santa Barbara, CA) (Fig. 1C). Bone slices were scanned using RTESPA-525 probes with a nominal spring constant of 200 N/m, and a nominal tip radius of 15–30 nm *via* subsequent zooming with the scan size changing from 20 μm, 5 μm, 1 μm, 500 nm, and 250 nm until the area of interest was identified. Images were acquired at the cantilever frequency of 2 kHz, scan rate of 0.5–1.0 Hz, and peak force setpoint was selected between 1 nN and 20 nN. The surface height, peak force error, DMTModulus, and adhesion channels were used to visually identify MCFs and EFM. Based on the images in the peak force error, DMTModulus and adhesion channels, MCFs (red arrows) and EFM (yellow arrows) regions could be readily distinguished (Fig. 1C). The round shaped MCFs with sizes ranging between 40 and 80 nm in diameter exhibited lower modulus and adhesion, while the surrounding EFM exhibited higher modulus and adhesion, filling in the space of 20–30 nm between the MCFs (Hassenkam et al., 2004). It is noteworthy that the aforementioned DMTModulus was determined using Derjaguin–Muller–Toporov (DMT) model, which is an alternative model for adhesive contact under small load, assuming that the contact profile remains the same as in Hertzian contact but with additional attractive interactions outside the area of contact for a spherical tip (Derjaguin et al., 1975; Muller et al., 1983). Thus, DMTModulus obtained from PeakForce QNM mapping was used only for identifying MCF and EFM in this study. The nanoindentation tests were performed under a much greater load (200 nN) using Oliver–Pharr method, which allows for different tip geometries, in order to ensure better measurements of both elastic modulus and energy dissipation during the tests.

2.3. Removal of GAGs

A protein deglycosylation mix (NC 1208546, New England Biolabs, Inc.) was utilized to remove the polysaccharides from PGs core proteins in bone matrix, which contained several enzymes required to remove all N-linked and simple O-linked glycans as well as some complex O-linked glycans (Wang et al., 2016). In brief, bone slices were washed with 1 × PBS twice, heated in a denaturing reaction buffer at 75 °C for 10 min to expose the GAGs in bone matrix. The slices were then immersed in 400 μl protein deglycosylation mix solution for 16 h at 37 °C. After the enzyme treatment, the bone slices were rinsed in distilled water three times each for 10 min in an ultrasonic water bath.

To confirm the efficacy of the aforementioned enzyme protocol in removing GAGs from bone matrix, an Alcian blue staining protocol described elsewhere (Melet et al., 1980) was used to estimate the amount of GAGs in bone matrix before and after the enzyme treatment (Fig. 2A). One bone slice each from the mid-diaphyseal femurs of the four donors was prepared, and then cut into two halves, one of which was stained without the enzyme treatment, while the other was stained after the enzyme treatment. Briefly, the bone slices were firstly polished and incubated in 3% acetic acid for 3 min, then stained in 1% Alcian blue 8GX (Sigma-Aldrich, St. Louis, MO, USA), and washed with 1 × PBS for three times each for 5 min. After the staining, the images of the stained bone slices were taken using a Keyence microscope (BZ-X710, Keyence, Osaka, Japan), and the staining intensity were analyzed using NIH Image J software to estimate the amount of GAGs in the bone matrix. The light intensity was analyzed from 4 to 6 fields within each specimen and averaged. The results indicated that GAGs were significantly reduced in the enzyme treated bone specimens compared with controls (Fig. 2B), thus verifying that the enzyme protocol did remove GAGs from bone matrix as expected.

It should be pointed out that due to the limited accessibility and penetration depth by the enzyme, the treatment might only remove GAGs from the surface of the specimens. Nonetheless, this would not influence the interpretation of AFM nanoindentation results since the average nanoindentation depth (<30 nm) was much less than the penetration depth of the enzyme (around 10 μm).

2.4. Determination of in situ mechanical properties of MCFs and EFM

The AFM ramping mode was used to measure the *in situ* nanoindentation behavior of MCFs and EFM. At the scan size of about 500 nm, MCFs and EFM regions could be identified from the AFM images and then the indentation test was performed on the selected MCFs and EFM with a force of 200 nN at a ramping size of 100 nm. The extent (loading) and retract (unloading) force-displacement curves were recorded, processed in Nanoscope Analysis software provided by Bruker, and exported for further processing and analysis.

The Elastic modulus of the sample (E) is calculated using the equation suggested by Oliver–Pharr method (Oliver and Pharr, 2004):

$$\frac{1-\nu^2}{E}=\frac{1}{E_r}-\frac{1-\nu_i^2}{E_i}, \tag{1}$$

where, E_r is the reduced modulus of the combined indenter sample system, E_i (=140 GPa) and ν_i (=0.265) are the Elastic modulus and Poisson's ratio for the indenter (silicon), ν (=0.3) is the estimated Poisson's ratio for the bone sample. Assuming an axisymmetric indenter, the reduced modulus can be calculated using

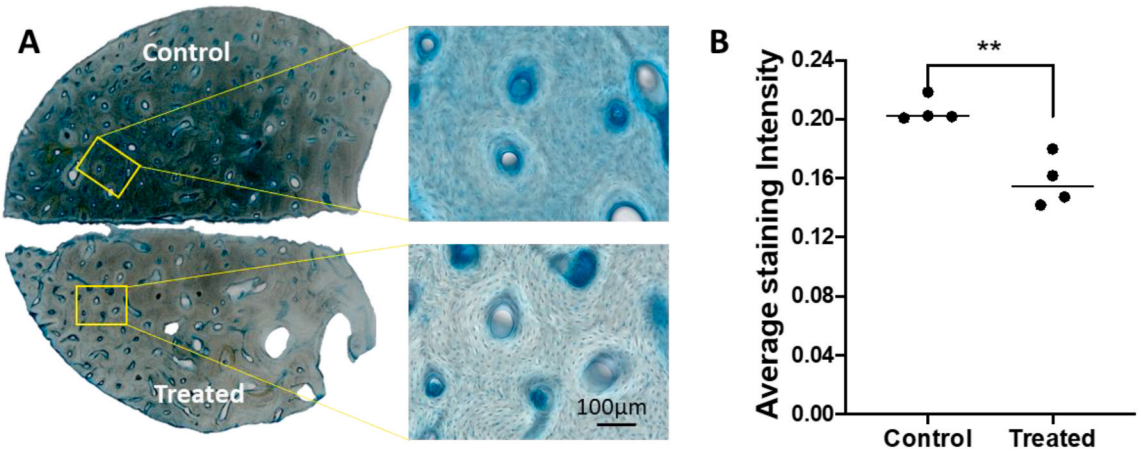

Fig. 2. Verification of GAGs removal using an Alcian Blue staining protocol. (A) Bone slices were cut into two halves, with one treated with protein deglycosylation mix and the other untreated. The two halves were then histochemically stained with Alcian Blue. (B) The staining images were taken and analyzed using NIH Image J software, and the stain density was quantified to estimate the amount of GAGs in bone matrix. Data shown are mean ± SD. N = 4. **p < 0.01. (For interpretation of the references to colour in this figure legend, the reader is referred to the Web version of this article.)

$$E_r = \frac{S\sqrt{\pi}}{2\sqrt{A_C}}\ , \tag{2}$$

where, S is the contact stiffness calculated as the slope at the inception of the unloading curve, which fits to the following power-law function.

$$F = B(h_{max} - h)^m\ , \tag{3}$$

with B and m as the constants to be determined. A_c is the projected contact area that can be estimated using the following equation, assuming the tip of indenter has a spherical shape

$$A_c = 2\pi R h_c - \pi h_c^2 \tag{4}$$

where R is the radius of the indenter tip, h_c is the contact depth over the perimeter of contact. Assuming pile-up is negligible during indentation, the elastic analysis (Sneddon, 1965) shows that

$$h_c = h_{max} - \varepsilon\frac{F_{max}}{S} \tag{5}$$

where, h_{max} is the maximum indentation depth (Fig. 3), and ε is a constant that depends on the indenter geometry, which is estimated as 0.75 for spherical tip to the first order approximation. To assess the post-yield behavior, we used an energy approach to estimate the capacity of MCFs and EFM in plastic energy dissipation. Briefly, the total elastic energy dissipation (U_e) was estimated as the area under the unloading curve, and the total plastic energy dissipation (U_p) was estimated as the area sandwiched between the extending and retracting curves (Fig. 3). Since the indentation depth (h_{max}) varied significantly ($p < 0.05$) with different test conditions (Fig. 4 and Table 1), the size of the deformed zone underneath the indenter would certainly be different. Thus, it is necessary to normalize the total energy dissipation with respect to the volume of deformed zone in order to estimate the capacity of MCFs and EFM in plastic energy dissipation. However, it is very challenging, if not impossible, to measure the volume of deformed zone (V_d) beneath the indentation. To address this issue, we used the ratio of U_p with respect to the total energy dissipation U_t (= U_e+ U_p) as a nominal measure ($u_p = U_p/U_t$) of the capacity of MCFs and EFM to dissipate plastic energy, assuming that u_p is equivalent to the plastic energy portion of the averaged strain energy density in the deformed zone ($u_p = \frac{U_p/V_d}{U/V_d}$). Using this measure, we expected to detect changes induced by GAGs removal

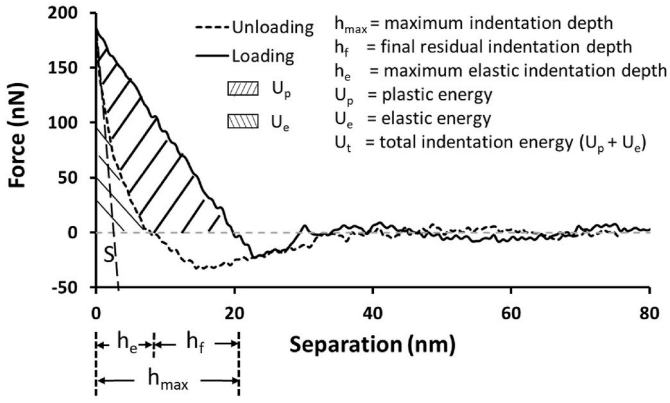

Fig. 3. Determination of elastic modulus (E) and energy dissipation during the AFM nanoindentation tests using the extending-retracting curves curve. E was calculated using Oliver-Pharr method, which requires the value of the slope of the unloading curve at the onset of unloading and the indentation depth. The plastic energy dissipation (U_p) during the nanoindentation was calculated from the area sandwiched between the loading and unloading curves and the elastic energy (U_e) was calculated from the area below the unloading curve above, respectively. The energy dissipation measurements were performed using the extending-retracting curves curve above zero indentation force.

in the plastic energy dissipation of MCFs and EFM.

2.5. Experimental consideration pertaining to effects of AFM probe radius and indentation depth

In this study, only new AFM probes, whose radius were between 8 and 12 nm, were used for nanoindentation tests in order to restrict each indentation test within the region of MCF (40–60 nm) and EFM (20 nm). In addition, deep indentation might compromise the sensitivity of the AFM test to capture the difference in the mechanical behavior between MCFs and EFM since the deformation zone underneath the indenter could encompass both MCFs and EFM regions. To alleviate the concern, the average nanoindentation depth was controlled to be less than 20 nm in this study to ensure that the nanoindentation test was confined in the target region (*i.e.*, MCF or EFM) as much as possible. Due to the possible error, however, only relative comparisons would be valid in this study to determine the differences between different test groups.

2.6. Statistical analysis

AFM measurements were performed at four different locations each in MCF and EFM regions, respectively, for each specimen. The results of each test group (N = 4) were presented as the mean ± standard deviation. Repeated measures ANOVA was performed to determine the effect of anatomic sites (*i.e.*, MCFs and EFM), matrix water (*i.e.*, wet and dry), and treatments (*i.e.*, baseline control, control, and GAGs removal) on the elastic modulus and plastic energy dissipation of bone. In addition, Tukey multiple comparisons were conducted between testing groups using GraphPad prism 8 statistical analysis software (Graphpad Prism). Statistically significant difference was considered only if $p < 0.05$. Asterisks indicate the degree of the statistical significance, *, $p < 0.05$; **, $p < 0.01$; ***, $p < 0.001$; and ****, $p < 0.0001$.

3. Results

3.1. AFM nanoindentation curve changed markedly among the test groups

The extending-retracting curves during the nanoindentation tests appeared to be significantly different under distinct test conditions (Fig. 4). First, the extending-retracting curves under the same indentation load (200 nN) changed markedly between the wet and dry conditions, showing that the maximum indentation depth (h_{max}) and the total energy dissipation (U_t) were much smaller under the dry condition than under the wet condition for both MCFs and EFM (Table 1). Next, the extending-retracting curves altered considerably before and after the removal of GAGs under the wet condition, revealing that the maximum indentation depth (h_{max}) and the total energy dissipation (U_t) decreased markedly ($p < 0.05$) after GAGs were removed in comparison to those of baseline control and control specimens (Table 1). For more details about the mechanical behavior of MCF and EFM, the elastic modulus (E) and the ratio of the plastic energy to total energy dissipation (u_p) were estimated from the extending-retracting curves of the AFM measurements, and the results were summarized in Table 1.

3.2. Water, treatments, and anatomic sites had marked effects on the mechanical behavior of bone

Three-way ANOVA analyses of the experimental results indicated that water (*i.e.*, wet and dry), treatments (*i.e.*, baseline control, control, and GAGs removal), and anatomic sites (*i.e.*, MCFs and EFM) all had significant effects on E and u_p of bone when these factors were considered individually (Table 2). Further analyses exhibited that the anatomic site had a cross-effect with treatments on u_p ($p < 0.05$), but not on$E$($p > 0.05$), and had an interactive effect with water only on E ($p < 0.0001$), but not on u_p ($p > 0.05$). Moreover, treatments and water had dependent

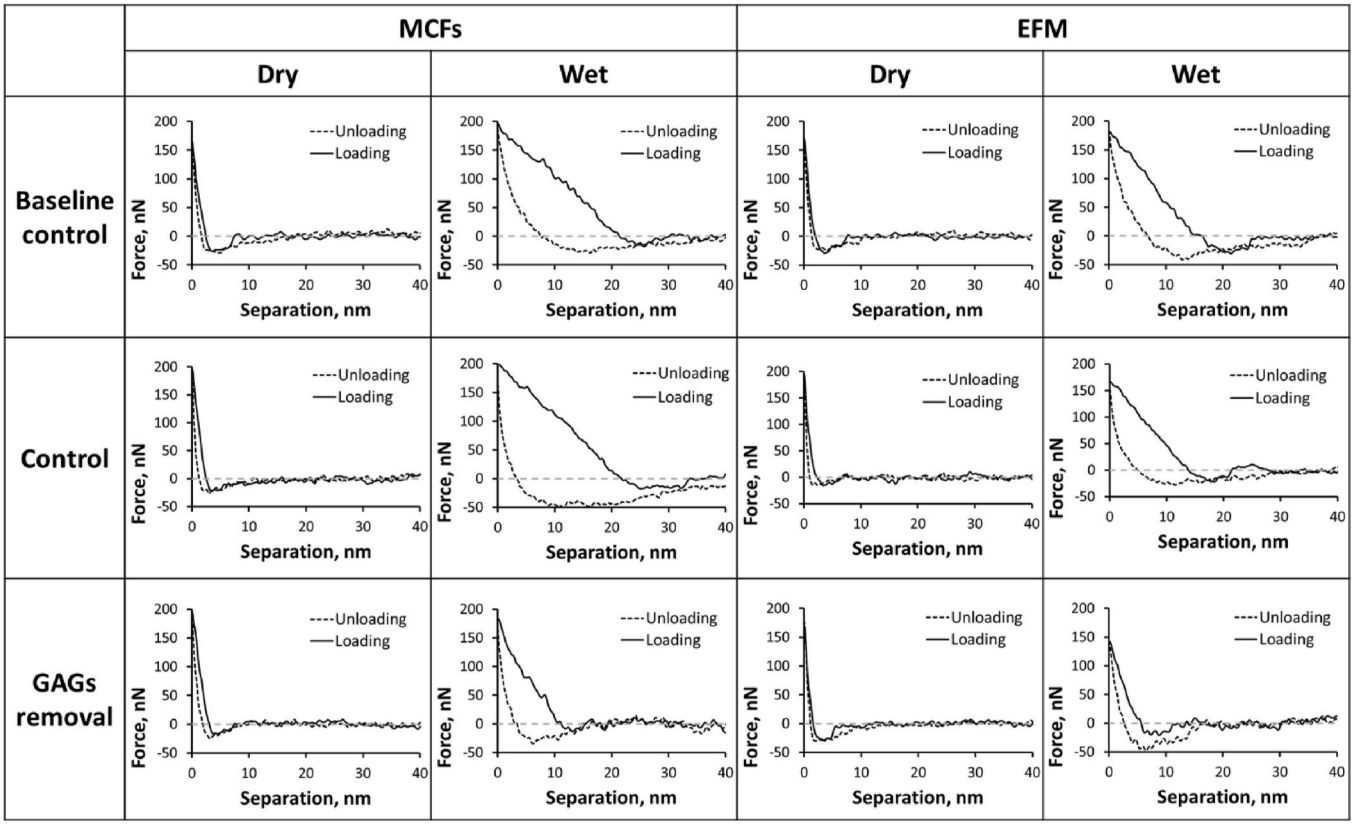

Fig. 4. Typical extending-retracting curves in AFM measurements obtained from bone samples of different test groups.

Table 1
AFM nanoindentation results under different conditions (N = 4).

		E (GPa)		u_p		h_{max} (nm)		U_t ($\times 10^{-15}$J)	
		MCF	EFM	MCF	EFM	MCF	EFM	MCF	EFM
Baseline control	Dry	9.74	14.0	0.556	0.449	3.33	2.66	0.279	0.201
		±1.04	±1.845	±0.089	±0.035	±0.630	±0.730	±0.070	±0.057
	Wet	1.51	2.03	0.702	0.628	19.6	16.0	1.84	1.35
		±0.295	±0.266	±0.006	±0.049	±1.72	±2.76	±0.291	±0.216
Control	Dry	10.7	14.6	0.587	0.543	2.74	2.17	0.275	0.219
		±0.536	±0.887	±0.044	±0.025	±0.545	±0.553	±0.038	±0.117
	Wet	2.02	2.44	0.870	0.845	19.2	14.0	2.011	1.31
		±0.087	±0.286	±0.035	±0.023	±3.20	±1.87	±0.008	±0.250
GAGs removal	Dry	9.88	13.9	0.570	0.495	3.54	2.58	0.262	0.209
		±2.27	±1.11	±0.037	±0.077	±1.10	±0.560	±0.079	±0.039
	Wet	2.78	3.80	0.674	0.497	11.3	6.50	0.959	0.562
		±0.707	±0.388	±0.054	±0.034	±1.58	±1.26	±0.250	±0.071

Table 2
Three-way repeated measures ANOVA analysis results.

Factors	Mechanical property	p value
Anatomic site	E	<0.0001
	u_p	<0.0001
Treatments	E	0.0103
	u_p	<0.0001
Water	E	<0.0001
	u_p	<0.0001
Anatomic site x Treatments	E	0.9269
	u_p	0.0062
Anatomic site x Water	E	<0.0001
	u_p	0.1409
Treatments x Water	E	0.0031
	u_p	<0.0001
Anatomic site x Treatments x Water	E	0.9667
	u_p	0.1945

effects on both E and $u_p$of bone ($p < 0.05$). Furthermore, these three factors had no cross-effect on u_p and E ($p > 0.05$) when their combined effect was considered. These results suggested that when considering the effect of the three factors (*i.e.*, matrix water, treatments, and anatomic sites) individually, their effects on the *in-situ E* and u_p were all significant. However, the effect of anatomic sites on E of bone appeared to be dependent on water, but independent on treatments when considering the interaction between these factors. More importantly, treatments and water had a coupling effect on the *in-situ* plastic energy dissipation (u_p) of the tissue, whereas their effects on u_p were independent of anatomic sites.

3.3. GAGs removal had significant effects on E of MCFs and EFM only in wet condition

Under the dry condition, the elastic modulus (E) did not show

significant changes ($p > 0.05$) among the baseline control, control, and GAGs removal groups, with 9.74 ± 1.04 GPa vs. 10.7 ± 0.536 GPa vs. 9.88 ± 2.27 GPa for MCFs, and 14.0 ± 1.845 GPa vs. 14.6 ± 0.887 GPa vs. 13.9 ± 1.11 GPa for EFM, respectively (Fig. 5). This result suggested that removal of GAGs had little effects on the elastic modulus of both MCFs and EFM after water was removed from the bone matrix. However, EFM appeared to be much stiffer than MCFs ($p < 0.01$). In comparison to dry condition, it was observed that E decreased almost in an order of magnitude ($p < 0.01$) under wet condition for all test groups (*i.e.*, baseline control, control, and GAGs removal) (Table 1), which was an unexpected result since the previous study showed that the elastic modulus of bone only changed about 20% from fully hydrated to completely dehydrated conditions (Nyman et al., 2006).

It was also noted that significant differences in E were observed between MCFs and EFM in baseline control, control, and GAGS removal specimens ($p < 0.01$), indicating that EFM was significantly stiffer than MCFs under the wet condition only when GAGs were removed ($p < 0.01$). These results suggested that GAGs removal had a significant effect on the elastic behavior of MCFs and EFM in presence of the matrix water. Moreover, it was observed that under the wet condition E of EFM increased significantly from 2.03 ± 0.266 GPa for baseline control specimens to 3.80 ± 0.388 GPa for GAGs removal specimens ($p < 0.0001$), while E of MCF also exhibited a similar trend (Fig. 5).

Comparing the baseline control and control groups, no significant differences were observed in E between MCF and EFM under both wet and dry conditions ($p > 0.05$), suggesting that the heating treatment had no significant effects on E in the two regions.

3.4. GAGs removal affected the plastic energy dissipation (u_p) only in EFM under the wet condition

The AFM nanoindentation tests under the dry condition indicated that u_p ($= U_p/U_t$) of MCFs and EFM did not change significantly among the baseline control, control, and GAGs removal specimens, suggesting that both heating and GAGs removal had little effects on the plastic energy dissipation in both MCFs and EFM when matrix water was removed (Fig. 6). However, without removal of GAGs, u_p of MCFs appeared to be little higher than that of EFM, suggesting that the capacity of MCF in dissipating plastic energy may be slightly more than EFM under both wet and dry conditions.

Under the wet condition, the multiple comparisons analyses indicated that u_p of MCFs did not change significantly between the baseline control and GAGs removal specimens ($p > 0.05$), whereas u_p of MCFs for the control specimens was significantly greater than the specimens in the other two groups ($p < 0.0001$) (Fig. 6). In contrast, u_p of EFM decreased about 21% from 0.628 ± 0.049 for the baseline control specimens to 0.497 ± 0.034 for the GAGs removal specimens ($p < 0.0001$) (Fig. 6). Similarly, u_p of EFM in the control specimens was significantly greater than those in the specimens of the other two groups ($p < 0.001$), suggesting that the heating treatment increased the capacity of MCFs and EFM in dissipating plastic energy.

In addition, it was observed that u_p of MCFs was similar to that of EFM ($p > 0.05$) when GAGs were not removed from the bone matrix (Fig. 6). These results indicated that the removal of GAGs affected plastic energy dissipation only in EFM, but not MCFs. However, the total energy dissipation (U_t) changed significantly with removal of GAGs for both MCF and EFM, corresponding to the varying indentation depth (h_{max}) in these compartments (Table 1).

4. Discussion

This study investigated the effect of GAGs removal on the *in-situ* mechanical properties of MCFs and EFM in human cortical bone samples using a high-resolution AFM system. The results of this study demonstrated that in the presence of matrix water, removal of GAGs significantly reduced the plastic energy dissipation capacity (u_p) of EFM, while having no significant influence on u_p of MCFs, thus supporting our hypothesis that coupling with water GAGs play a pivotal role in plastic energy dissipation in EFM.

In this study, the high-resolution AFM techniques enabled us to identify MCFs and EFM at the nanoscopic length scales. The diameter of MCFs observed in this study varied between 40 and 60 nm as shown in the peak force error mapping (Fig. 1C), which is comparable with those reported in the literature. For example, previous studies report that the diameter of collagen fibrils ranges between 30 and 100 nm in human bone, 43.1 ± 9.9 nm in rabbit femurs and 39.5 ± 6.5 nm in rat femurs

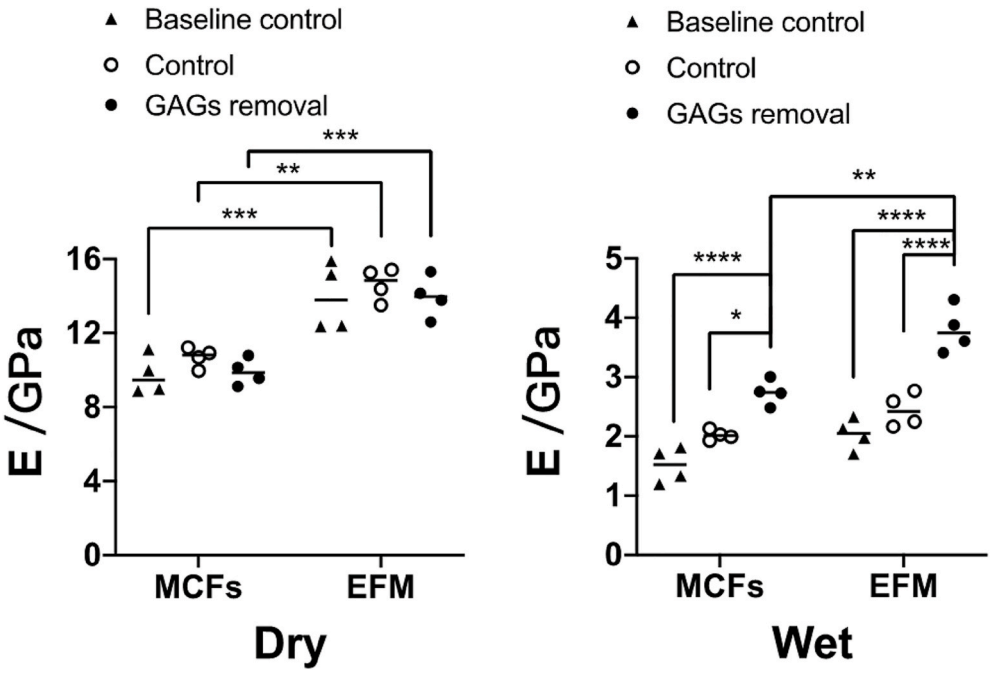

Fig. 5. The effects of GAGs removal on the elastic modulus (E) of both MCF and EFM under dry and wet conditions. Baseline control: no treatments; Control: heating without enzyme treatment, GAGs removal: heating + enzyme treatment to remove GAGs. *, $p < 0.05$; **, $p < 0.01$; ***, $p < 0.001$; ****, $p < 0.0001$.

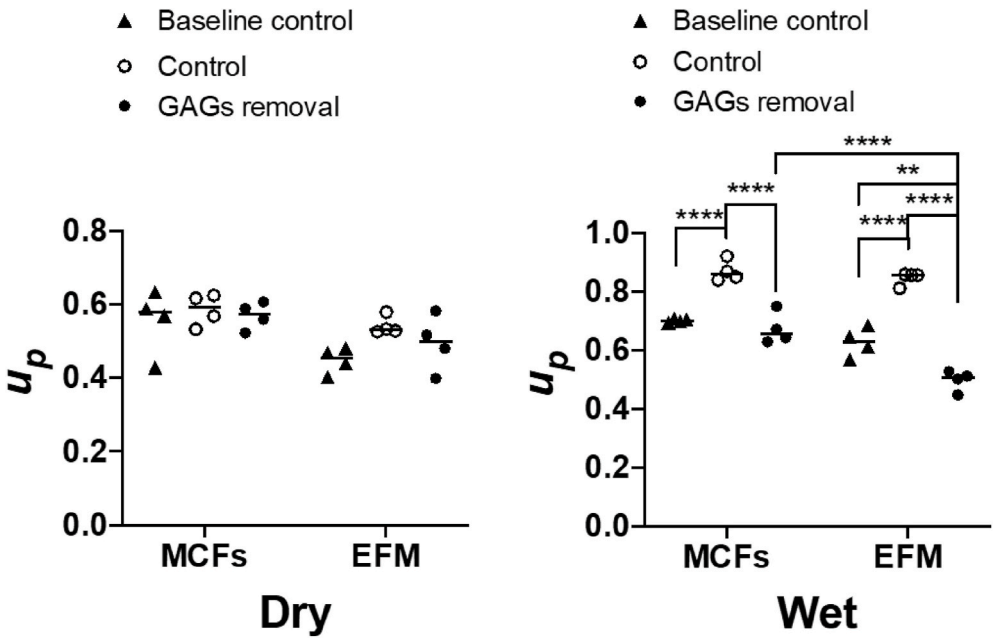

Fig. 6. The effects of GAGs removal on the plastic energy dissipation (up) of both MCF and EFM under dry and wet conditions. Baseline control: no treatments; Control: heating without enzyme treatment, GAGs removal: heating + enzyme treatment to remove GAGs. *, $p < 0.05$; **, $p < 0.01$; ***, $p < 0.001$; ****, $p < 0.0001$.

(Barth et al., 2011; Berillis et al., 2006; Starborg et al., 2013; Tzaphlidou, 2008b). In addition, the DMTModulus mapping (Fig. 1C) indicated that EFM was stiffer than MCFs. This is not surprising because the collagen phase, which is dominant in MCFs (Tzaphlidou, 2008a), is much more compliant than bone mineral crystals, which are the major component of EFM (Pidaparti et al., 1996). Moreover, the corresponding adhesion mapping (Fig. 1C) indicated that the silicon probe had a weaker adhesion to MCFs than to EFM, thus further confirming the material difference between the two ultrastructural compartments in bone. All of the aforementioned measurements have helped visually distinguish between MCFs and EFM, thus allowing for the later nanoindentation tests to determine their mechanical behavior individually.

The high-resolution AFM techniques also allowed for measuring the *in situ* mechanical behavior of MCFs and EFM separately. The Elastic modulus (E) of MCFs in the longitudinal direction was measured as 1.51 ± 0.295 GPa under the wet condition. These values are comparable with those (1.2–1.5 GPa) reported in a previous study on human tooth samples tested in the transverse direction using AFM nanoindentation tests and Sneddon's formulation for a cylindrical cone indenter (Balooch et al., 2008). It is noteworthy that the elastic modulus of MCFs measured using AFM techniques appears to be much lower than those obtained from other techniques, including *in silico* simulations. For example, a small angle X-ray scattering (SAXS) study by Almer and Stock (2007) using synchrotron sources reported that E of MCFs in its longitudinal direction was 18.3 GPa for cortical bone samples from canine fibula tested under wet condition (Almer and Stock, 2007), whereas an *in-silico* study predicted that the elastic modulus of MCFs was between 19.1 and 20.5 GPa in the longitudinal direction (Yuan et al., 2011). Interestingly, these values are close to those (9.74 ± 1.04 GPa) measured under the dehydrated condition in this study.

In addition, AFM nanoindentation tests showed that EFM appeared to be stiffer than MCFs, which was also indicated in the DMTModulus mapping image (Fig. 1C). It is commonly believed that EFM consists of non-collagenous proteins (including proteoglycans) and mineral crystals (Boskey et al., 1991; Hashimoto et al., 1995b; Mbuyi-Muamba et al., 1989b; Waddington et al., 2003). However, the results from the previous studies are controversial and inconsistent regarding mineral distributions inside and outside of collagen fibrils in bone. Some researchers believe that 75% of mineral crystals resided outside MCFs (Pidaparti et al., 1996), while others deem that EFM contains only a small portion of total mineral content (<25%) (Katz and Li, 1973). Since mineral content is strongly correlated with the elastic modulus of bone (Currey, 1988), the results of our study agree more with the notion that more minerals reside in EFM than in MCFs, thus making EFM much stiffer than MCFs.

AFM measurements of this study unexpectedly indicate that the elastic modulus (E) of both MCFs and EFM changed in an order of magnitude from wet to dry conditions ($p < 0.0001$). If it were true, similar changes would be reflected in the mechanical property of bone at higher hierarchical levels. However, previous studies showed that the elastic modulus of bulk bone tissue tested under dry condition increased by less than 20% compared to that obtained under wet conditions (Nyman et al., 2006). In fact, it should not be the matrix water but the mineral phase that determine the elastic modulus of bone. The following possible scenarios could be considered to explain the discrepancy. First, the contact area function required by the Oliver-Pharr method is very sensitive to the indenter geometry and indentation depth. Since the indentation depth is much greater on the hydrated bone samples than on the dehydrated ones, it is possible that the elastic modulus is underestimated for the hydrated bone samples (Kontomaris and Malamou, 2020; Mc Elhaney et al., 1998; Pharr et al., 1992). In fact, similar trend was also observed in the previous AFM studies, showing that the elastic modulus of dehydrated MCFs was 7.9 ± 2.8 GPa, while hydration tremendously decreased its modulus to 3.3 ± 0.5 MPa (Andriotis et al., 2015; Hengsberger et al., 2002). Second, it is possible that the mechanical behavior of bone at the nanoscopic length scale is different from that at the microscopic (or tissue) levels. It is commonly agreed that D spacing of mineralized collagen fibrils in bone is about 67 nm and the size of mineral crystallites is also in a similar dimension (~1–5 nm in thickness, ~10–40 nm in width, and ~20–100 nm in length) (Adele, 2003; Boskey and Myers, 2004; Hassenkam et al., 2004), which are comparable to or even greater than the radius of the indenter (20–30 nm). Thus, the AFM nanoindentation may be unable to capture the mechanical behavior of whole MCFs and EFM, but the local behavior of the two compartments. Further investigation is needed to address this important issue.

It was noted in this study that heating bone in a denaturation reaction buffer at 75 °C for 10 min would increase the capacity of MCF and

EFM in plastic energy dissipation during the nanoindentation test on the control specimens (Fig. 6 and Table 1). This heating treatment was used to expose GAGs by unraveling surrounding proteins without damaging collagen fibrils so that the enzyme treatment could quickly remove GAGs from their core proteins. A possible explanation for this heating effect is that unraveling proteins may create additional spaces for the existing GAGs to attract more water into bone matrix, thus facilitating plastic energy dissipation during the nanoindentation test. As a result, the capacity of MCF and EFM in plastic energy dissipation would be enhanced. However, removal of GAGs would lead to water loss in bone matrix, especially in EFM, thus causing more reduction in plastic energy dissipation in EFM regions.

Another new finding of this study is that water has significant effects on plastic energy dissipation in both EFM and MCF. In addition, the capacity of EFM in plastic energy dissipation appears to be comparable with that of MCFs. In the past, the collagen phase is commonly considered as the major contributor to the toughness of bone (Ritchie et al., 2009), whereas the contribution of EFM is largely overlooked. The results of this study, for the first time, suggest that EFM is another major contributor to the toughness of bone and very sensitive to its hydration status. Based on the concept of theoretical fiber volume fraction (Endruweit et al., 2013), greater than 30% volume of bone would be comprised of EFM since MCFs are packed randomly with varying diameters. Therefore, any changes in the mechanical properties of EFM would be reflected in the bulk behavior of bone. Since NCPs, which are highly hydrophilic for extracting and retaining water and most likely reside in EFM rather than MCFs, loss of water would stiffen NCPs, thus subsequently reducing the capacity of EFM in dissipating plastic energy.

Removal of GAGs appears to impose significant effects on the mechanical behavior of both MCFs and EFM only under the hydrated condition, thus suggesting a coupling effect of GAGs with bound water in toughening bone matrix. Previous studies have indicated that GAGs play an important role in toughening bone tissue (Hua et al., 2020; Wang et al., 2016). However, which ultrastructural compartment (*e.g.*, MCFs, or EFM, or both) is affected by GAGs is still unknown. This study has, for the first time, addressed this question, showing that GAGs, coupling with water, only affect the capacity of EFM in plastic energy dissipation (u_p), whereas removal of GAGs appears to have little effects on u_p of MCFs. By removing the matrix water, however, the effect of GAGs on u_p of EFM diminishes. These results suggest that GAGs are most likely present only in EFM, which is consistent with the results reported in the literature (Mbuyi-Muamba et al., 1989b). It is worth mentioning that u_p is by no means a measure of toughness, but an indirect estimate of plastic energy dissipation during the nanoindentation tests. Nonetheless, this measure is still useful for relative comparisons between MCFs and EFM in their plastic energy dissipation capacity before and after removal of GAGs from the bone matrix.

Interestingly, the results of this study indicated that removal of GAGs appeared to have significant effect on E for both MCFs and EFM, showing that E increased in the two compartments after GAGs were removed from the bone matrix. This result is unexpected since the organic phase is commonly deemed to have limited effects on bone stiffness (Yuan et al., 2011). One possible explanation for its effect on EFM is that loss of bound water induced by removal of GAGs may cause shrinking and hardening of the organic interfaces between the extrafibrillar minerals, thus leading to stiffening of EFM. As a result, MCF may be also stiffened due to the stiffening of surrounding EFM. Further investigation is needed to unravel its underlying mechanism.

The aforementioned findings may have the following clinical and biological significances. First, understanding the role of MCFs and EFM in plastic energy dissipation of bone gives rise to new insights in nanomechanics of bone. Second, the finding that GAGs, coupling with water, play a marked role in regulating the plastic energy dissipation of EFM provides a potential mechanistic pathway for age-related deterioration of bone tissue quality due to loss of GAGs (Wang et al., 2018). Third, deterring or preventing GAGs loss in bone matrix may be a potential strategy for treating age-related bone fragility fractures. Finally, this study offers potentials of AFM nanoindentation techniques in testing biological materials like bone.

There are several other limitations of this study. First, bone samples are obtained from a very limited sample population (*i.e.*, mid-aged female and mid-diaphyseal femurs). Further investigation using more inclusive sample populations is required to confirm the outcome of this study. Second, since the radius of nanoindenter used in study is between 20 and 30 nm, the size of indentation would be very close to the diameter of MCFs (40–60 nm) and even larger than the size of EFM regions (<20 nm) when large indentation depths are reached under the wet condition (*e.g.*, $h_{max}/R \rightarrow 0.7$). It is well known that the size of the deformation zone underneath an indenter is much larger than the size of surface indentation impression. Therefore, both MCFs and EFM regions would be involved in the indentation deformation if h_{max}/R is large. Because of this, the results of AFM indentation tests are only suitable for relative comparisons, especially when testing the bone specimens under the wet condition. Third, the spherical tip was assumed in this study, while in reality the geometry of the sharp AFM tip used in this study was not well-defined. Finally, it should be noted that the wet and dry status of the tissue tested in this study might not necessarily reflect physiologically relevant variations of bound water in bone.

5. Conclusions

Using high-resolution AFM techniques, this study investigated the effect of removal of GAGs on the *in situ* mechanical properties of EFM and MCFs in human cadaver bone samples. The results indicate that both MCFs and EFM significantly contribute to the plastic energy dissipation in bone, and that removal of GAGs, coupling with matrix water, may significantly reduce the capacity of EFM, but not MCFs, in plastic energy dissipation. Although there are some limitations, this study, for the first time, differentiates the contributions of MCFs and EFM to the *in situ* mechanical behavior of bone, and reveals the role of GAGs in regulating the *in situ* mechanical properties of bone.

Author statement

Yan Han: Investigation; Data curation; Validation; Formal analysis; Methodology; Roles/Writing - original draft. **Joel Gomez**: Data curation; Investigation; Formal analysis; Validation. **Rui Hua**: Data curation; Investigation; Formal analysis; Validation; Writing - review & editing. **Pengwei Xiao**: Formal analysis; Writing - review & editing. **Wei Gao**: Methodology; Resources; Software; Supervision; Funding acquisition; Writing - review & editing. **Jean X. Jiang**: Conceptualization; Formal analysis; Resources; Methodology; Supervision; Funding acquisition; Writing - review & editing. **Xiaodu Wang**: Conceptualization; Formal analysis; Methodology; Resources; Supervision; Roles/Writing - original draft; Writing - review & editing; Funding acquisition; Project administration.

Declaration of competing interest

The authors declare that they have no known competing financial interests or personal relationships that could have appeared to influence the work reported in this paper.

Acknowledgment

Research reported in this study was supported by National Institute of Arthritis, Musculoskeletal and Skin Diseases of the National Institutes of Health under award number R01AR076190 to XDW and JXJ and Welch Foundation grant AQ-1507 to JXJ. The content is solely the responsibility of the authors and does not necessarily represent the official views of the National Institutes of Health.

References

Adele, B., 2003. Bone mineral crystal size. Osteoporos. Int. 14, 16–21.

Almer, J.D., Stock, S.R., 2007. Micromechanical response of mineral and collagen phases in bone. J. Struct. Biol. 157, 365–370.

Andriotis, O., Chang, S., Vanleene, M., Howarth, P., Davies, D., Shefelbine, S., Buehler, M., Thurner, P., 2015. Structure–mechanics relationships of collagen fibrils in the osteogenesis imperfecta mouse model. J. R. Soc. Interface 12, 20150701.

Bailey, S., Karsenty, G., Gundberg, C., Vashishth, D., 2017. Osteocalcin and osteopontin influence bone morphology and mechanical properties. Ann. N. Y. Acad. Sci. 1409, 79–84.

Balooch, M., Habelitz, S., Kinney, J.H., Marshall, S.J., Marshall, G.W., 2008. Mechanical properties of mineralized collagen fibrils as influenced by demineralization. J. Struct. Biol. 162, 404–410.

Barth, H.D., Zimmermann, E.A., Schaible, E., Tang, S.Y., Alliston, T., Ritchie, R.O., 2011. Characterization of the effects of x-ray irradiation on the hierarchical structure and mechanical properties of human cortical bone. Biomaterials 32, 8892–8904.

Berillis, P., Emfietzoglou, D., Tzaphlidou, M., 2006. Collagen fibril diameter in relation to bone site and to calcium/phosphorus ratio. TheScientificWorldJOURNAL 6, 1109–1113.

Boskey, A.L., 1992. Mineral-matrix interactions in bone and cartilage. Clin. Orthop. Relat. Res. 244–274.

Boskey, A.L., Maresca, M., Wikstrom, B., Hjerpe, A., 1991. Hydroxyapatite formation in the presence of proteoglycans of reduced sulfate content: studies in the brachymorphic mouse. Calcif. Tissue Int. 49, 389–393.

Boskey, A.L., Myers, E.R., 2004. Is bone mineral crystal size a significant contributor to" bone quality"? IBMS BoneKEy 1, 4.

Burr, D.B., 2002. The contribution of the organic matrix to bone's material properties. Bone 31, 8–11.

Currey, J.D., 1984a. Effects of differences in mineralization on the mechanical properties of bone. Phil. Trans. Roy. Soc. Lond. B Biol. Sci. 304, 509–518.

Currey, J.D., 1984b. What should bones be designed to do? Calcif. Tissue Int. 36 (Suppl. 1), S7–S10.

Currey, J.D., 1988. The effects of drying and re-wetting on some mechanical properties of cortical bone. J. Biomech. 21, 439–441.

Derjaguin, B.V., Muller, V.M., Toporov, Y.P., 1975. Effect of contact deformations on the adhesion of particles. J. Colloid Interface Sci. 53, 314–326.

Endruweit, A., Gommer, F., Long, A., 2013. Stochastic analysis of fibre volume fraction and permeability in fibre bundles with random filament arrangement. Compos. Appl. Sci. Manuf. 49, 109–118.

Fisher, L.W., Termine, J., Dejter Jr., S., Whitson, S., Yanagishita, M., Kimura, J., Hascall, V., Kleinman, H., Hassell, J., Nilsson, B., 1983. Proteoglycans of developing bone. J. Biol. Chem. 258, 6588–6594.

Fratzl, P., Weinkamer, R., 2007. Nature's hierarchical materials. Prog. Mater. Sci. 52, 1263–1334.

Garcia, R., 2020. Nanomechanical mapping of soft materials with the atomic force microscope: methods, theory and applications. Chem. Soc. Rev. 49, 5850–5884.

Goldberg, M., Takagi, M., 1993. Dentine proteoglycans: composition, ultrastructure and functions. Histochem. J. 25, 781–806.

Hang, F., Barber, A.H., 2011. Nano-mechanical properties of individual mineralized collagen fibrils from bone tissue. J. R. Soc. Interface 8, 500–505.

Hashimoto, Y., Lester, G., Caterson, B., Yamauchi, M., 1995a. EDTA-insoluble, calcium-binding proteoglycan in bovine bone. Calcif. Tissue Int. 56, 398–402.

Hashimoto, Y., Lester, G.E., Caterson, B., Yamauchi, M., 1995b. EDTA-insoluble, calcium-binding proteoglycan in bovine bone. Calcif. Tissue Int. 56, 398–402.

Hassenkam, T., Fantner, G.E., Cutroni, J.A., Weaver, J.C., Morse, D.E., Hansma, P.K., 2004. High-resolution AFM imaging of intact and fractured trabecular bone. Bone 35, 4–10.

Hengsberger, S., Kulik, A., Zysset, P., 2002. Nanoindentation discriminates the elastic properties of individual human bone lamellae under dry and physiological conditions. Bone 30, 178–184.

Hua, R., Ni, Q., Eliason, T.D., Han, Y., Gu, S., Nicolella, D.P., Wang, X., Jiang, J.X., 2020. Biglycan and chondroitin sulfate play pivotal roles in bone toughness via retaining bound water in bone mineral matrix. Matrix Biol. : journal of the International Society for Matrix Biology 94, 95–109.

Iozzo, R.V., Schaefer, L., 2015. Proteoglycan form and function: a comprehensive nomenclature of proteoglycans. Matrix Biol. 42, 11–55.

Jameson, M.W., Hood, J.A., Tidmarsh, B.G., 1993. The effects of dehydration and rehydration on some mechanical properties of human dentine. J. Biomech. 26, 1055–1065.

Katz, E.P., Li, S.T., 1973. Structure and function of bone collagen fibrils. J. Mol. Biol. 80, 1–15.

Kontomaris, S., Malamou, A., 2020. Hertz model or Oliver & Pharr analysis? Tutorial regarding AFM nanoindentation experiments on biological samples. Mater. Res. Express 7, 033001.

Lamoureux, F., Baud'huin, M., Duplomb, L., Heymann, D., Rédini, F., 2007. Proteoglycans: key partners in bone cell biology. Bioessays 29, 758–771.

Maghsoudi-Ganjeh, M., Wang, X., Zeng, X., 2020. Computational investigation of the effect of water on the nanomechanical behavior of bone. Journal of the mechanical behavior of biomedical materials 101, 103454.

Mbuyi-Muamba, J., Dequeker, J., Gevers, G., 1989a. Collagen and non-collagenous proteins in different mineralization stages of human femur. Cells Tissues Organs 134, 265–268.

Mbuyi-Muamba, J.M., Dequeker, J., Gevers, G., 1989b. Collagen and non-collagenous proteins in different mineralization stages of human femur. Acta Anat. 134, 265–268.

Mc Elhaney, K., Vlassak, J.J., Nix, W.D., 1998. Determination of indenter tip geometry and indentation contact area for depth-sensing indentation experiments. J. Mater. Res. 13, 1300–1306.

Melet, J., Hooghwinkel, G., Giesberts, M., Van Gelderen, H., 1980. A semi-quantitative micromethod for the determination of free glycosaminoglycans in serum. Results from studies on serum of healthy children of various age and patients affected by mucopolysaccharidosis. Clin. Chim. Acta 108, 179–188.

Morgan, S., Poundarik, A.A., Vashishth, D., 2015. Do non-collagenous proteins affect skeletal mechanical properties? Calcif. Tissue Int. 97, 281–291.

Muller, V., Derjaguin, B., Toporov, Y.P., 1983. On two methods of calculation of the force of sticking of an elastic sphere to a rigid plane. Colloid. Surface. 7, 251–259.

Nalla, R.K., Kinney, J.H., Ritchie, R.O., 2003. Mechanistic fracture criteria for the failure of human cortical bone. Nat. Mater. 2, 164–168.

Nyman, J.S., Roy, A., Shen, X., Acuna, R.L., Tyler, J.H., Wang, X., 2006. The influence of water removal on the strength and toughness of cortical bone. J. Biomech. 39, 931–938.

Oliver, W.C., Pharr, G.M., 2004. Measurement of hardness and elastic modulus by instrumented indentation: advances in understanding and refinements to methodology. J. Mater. Res. 19, 3–20.

Pharr, G., Oliver, W., Brotzen, F., 1992. On the generality of the relationship among contact stiffness, contact area, and elastic modulus during indentation. J. Mater. Res. 7, 613–617.

Pidaparti, R.M., Chandran, A., Takano, Y., Turner, C.H., 1996. Bone mineral lies mainly outside collagen fibrils: predictions of a composite model for osteonal bone. J. Biomech. 29, 909–916.

Reilly, G.C., Knapp, H.F., Stemmer, A., Niederer, P., Tate, M.L.K., 2001. Investigation of the morphology of the lacunocanalicular system of cortical bone using atomic force microscopy. Ann. Biomed. Eng. 29, 1074–1081.

Rho, J.-Y., Kuhn-Spearing, L., Zioupos, P., 1998. Mechanical properties and the hierarchical structure of bone. Med. Eng. Phys. 20, 92–102.

Ritchie, R.O., Buehler, M.J., Hansma, P., 2009. Plasticity and Toughness in Bone.

Samuel, J., Sinha, D., Zhao, J.C.-G., Wang, X., 2014. Water residing in small ultrastructural spaces plays a critical role in the mechanical behavior of bone. Bone 59, 199–206.

Sroga, G.E., Vashishth, D., 2012. Effects of bone matrix proteins on fracture and fragility in osteoporosis. Curr. Osteoporos. Rep. 10, 141–150.

Starborg, T., Kalson, N.S., Lu, Y., Mironov, A., Cootes, T.F., Holmes, D.F., Kadler, K.E., 2013. Using transmission electron microscopy and 3 View to determine collagen fibril size and three-dimensional organization. Nat. Protoc. 8, 1433.

Tzaphlidou, M., 2008a. Bone architecture: collagen structure and calcium/phosphorus maps. J. Biol. Phys. 34, 39–49.

Tzaphlidou, M., 2008b. Bone architecture: collagen structure and calcium/phosphorus maps. J. Biol. Phys. 34, 39–49.

Waddington, R.J., Roberts, H.C., Sugars, R.V., Schonherr, E., 2003. Differential roles for small leucine-rich proteoglycans in bone formation. Eur. Cell. Mater. 6, 12–21 discussion 21.

Wang, Q., Wang, M.-h., Wang, K.-f., Liu, Y., Zhang, H.-p., Lu, X., Zhang, X.-d., 2015. Computer simulation of biomolecule–biomaterial interactions at surfaces and interfaces. Biomed. Mater. 10, 032001.

Wang, X., 2002. Age-related changes in the collagen network and toughness of bone. Bone 31, 1–7.

Wang, X., Bank, R.A., TeKoppele, J.M., Agrawal, C.M., 2001. The role of collagen in determining bone mechanical properties. J. Orthop. Res. 19, 1021–1026.

Wang, X., Hua, R., Ahsan, A., Ni, Q., Huang, Y., Gu, S., Jiang, J.X., 2018. Age-related deterioration of bone toughness is related to diminishing amount of matrix glycosaminoglycans (Gags). JBMR plus 2, 164–173.

Wang, X., Xu, H., Huang, Y., Gu, S., Jiang, J.X., 2016. Coupling effect of water and proteoglycans on the in situ toughness of bone. J. Bone Miner. Res. 31, 1026–1029.

Weiner, S., Wagner, H.D., 1998. The material bone: structure-mechanical function relations. Annu. Rev. Mater. Sci. 28, 271–298.

Wise, E.R., Maltsev, S., Davies, M.E., Duer, M.J., Jaeger, C., Loveridge, N., Murray, R.C., Reid, D.G., 2007. The organic– mineral interface in bone is predominantly polysaccharide. Chem. Mater. 19, 5055–5057.

Yang, P.-F., Nie, X.-T., Zhao, D.-D., Wang, Z., Ren, L., Xu, H.-Y., Rittweger, J., Shang, P., 2018. Deformation regimes of collagen fibrils in cortical bone revealed by in situ morphology and elastic modulus observations under mechanical loading. Journal of the mechanical behavior of biomedical materials 79, 115–121.

Yuan, F., Stock, S.R., Haeffner, D.R., Almer, J.D., Dunand, D.C., Brinson, L.C., 2011. A new model to simulate the elastic properties of mineralized collagen fibril. Biomech. Model. Mechanobiol. 10, 147–160.

Zhu, P., Xu, J., Sahar, N., Morris, M.D., Kohn, D.H., Ramamoorthy, A., 2009. Time-resolved dehydration-induced structural changes in an intact bovine cortical bone revealed by solid-state NMR spectroscopy. J. Am. Chem. Soc. 131, 17064–17065.